Analyst

PAPER

View Article Online
View Journal

Cite this: DOI: 10.1039/c9an00532c

Smartphone-imaged microfluidic biochip for measuring CD64 expression from whole blood†

Tanmay Ghonge,[a,b,c] Hatice Ceylan Koydemir,[d] Enrique Valera,[a,b,c] Jacob Berger,[a,b,c] Carlos Garcia,[a,b,c] Noshin Nawar,[a,b,c] Justin Tiao,[a,b,c] Gregory L. Damhorst,[e] Anurup Ganguli,[a,b] Umer Hassan,[f] Aydogan Ozcan *[d,g,h] and Rashid Bashir *[a,b,c,i]

Sepsis, a life-threatening syndrome that contributes to millions of deaths annually worldwide, represents a moral and economic burden to the healthcare system. Although no single, or even a combination of biomarkers has been validated for the diagnosis of sepsis, multiple studies have shown the high specificity of CD64 expression on neutrophils (nCD64) to sepsis. The analysis of elevated nCD64 in the first 2–6 hours after infection during the pro-inflammatory stage could significantly contribute to early sepsis diagnosis. Therefore, a rapid and automated device to periodically measure nCD64 expression at the point-of-care (POC) could lead to timely medical intervention and reduced mortality rates. Current accepted technologies for measuring nCD64 expression, such as flow cytometry, require manual sample preparation and long incubation times. For POC applications, however, the technology should be able to measure nCD64 expression with little to no sample preparation. In this paper, we demonstrate a smartphone-imaged microfluidic biochip for detecting nCD64 expression in under 50 min. In our assay, first unprocessed whole blood is injected into a capture chamber to immunologically capture nCD64 along a staggered array of pillars, which were previously functionalized with an antibody against CD64. Then, an image of the capture channel is taken using a smartphone-based microscope. This image is used to measure the cumulative fraction of captured cells (γ) as a function of length in the channel. During the image analysis, a statistical model is fitted to γ in order to extract the probability of capture of neutrophils per collision with a pillar (ε). The fitting shows a strong correlation with nCD64 expression measured using flow cytometry (R^2 = 0.82). Finally, the applicability of the device to sepsis was demonstrated by analyzing nCD64 from 8 patients (37 blood samples analyzed) along the time they were admitted to the hospital. Results from this analysis, obtained using the smartphone-imaged microfluidic biochip were compared with flow cytometry. Again, a correlation coefficient R^2 = 0.82 (slope = 0.99) was obtained demonstrating a good linear correlation between the two techniques. Deployment of this technology in ICU could significantly enhance patient care worldwide.

Received 22nd March 2019,
Accepted 8th May 2019

DOI: 10.1039/c9an00532c

rsc.li/analyst

1. Introduction

Sepsis, a clinical syndrome defined as a life-threatening organ dysfunction caused by a dysregulated host response to infection,[1] represents a moral and economic burden to the healthcare system. Sepsis is a leading cause of mortality worldwide and is also the most expensive condition treated in hospitals in the United States,[2,3] costing the U.S. healthcare system more than $23 billion in 2013.[4] Clinical diagnosis of sepsis is challenging given the vast heterogeneity of clinical presentation.[5] Over the last 30 years, clinics have used different criteria such as systemic inflammatory response syndrome (SIRS), Logistic Organ Dysfunction System (LODS) and Sequential Organ Failure Assessment (SOFA) or quick SOFA (qSOFA) as screening tools to assess the severity of organ dys-

[a]Department of Bioengineering, University of Illinois at Urbana-Champaign, Urbana, IL 61801, USA. E-mail: rbashir@illinois.edu
[b]Micro and Nanotechnology Lab, University of Illinois at Urbana-Champaign, Urbana, IL 61801, USA
[c]Biomedical Research Center, Carle Foundation Hospital, Urbana, IL, 61801, USA
[d]Electrical and Computer Engineering, University of California, Los Angeles, CA, 90095, USA. E-mail: ozcan@ucla.edu
[e]Emory University School of Medicine, Emory University, Atlanta, GA, 30322, USA
[f]Department of Electrical and Computer Engineering, Rutgers University, Piscataway, NJ, 08854, USA
[g]Bioengineering, University of California, Los Angeles, CA, 90095, USA
[h]California NanoSystems Institute, University of California, Los Angeles, CA, 90095, USA
[i]Carle Illinois College of Medicine, Urbana, IL, 61801, USA

†Electronic supplementary information (ESI) available. See DOI: 10.1039/c9an00532c

function in a potentially septic patient.[1,6] Common factors among these criteria are non-specificity and very high false positive rates. Although other tests, such as blood cultures, are also used to detect bacteremia and to help in the diagnosis of sepsis, currently there is no single gold standard test to diagnose this condition.[7] Additional challenges include the increasing mortality rate with delays in treatment, as survival rates have been reported to drop by 7.6% every hour that the proper antibiotics are not administered.[8] This is especially critical considering that blood cultures can take several days to provide definitive results for absence of bacteria and have a 40% false negative ratio.[9] In fact, in a recent surveillance study of sepsis in U.S. hospitals including over 140 000 patients, only 17.2% had positive bacterial blood culture results.[10]

Measurement of circulating biomarkers has been proposed as a faster route for prognosis, stratification, diagnosis, and monitoring of sepsis.[11] A host of serum proteins such as C-Reactive Protein (CRP), Procalcitonin (PCT), and Interleukin 6 (IL-6), may be useful to diagnose sepsis in its early phase.[12–14] Neutrophil activation has also been suggested as a marker for sepsis diagnosis and monitoring. For example, some studies have linked elevated expression of CD64 on neutrophils (nCD64) to the onset of sepsis,[15,16] as this biomarker spikes in the first 2–6 hours after infection during the pro-inflammatory stage. It was also reported that neonates suspected of sepsis have significantly higher nCD64 compared with controls subjects.[17] A meta-analysis of 26 studies including 3944 patients found that nCD64 expression measurements could lead to early diagnosis of sepsis with 76% sensitivity and 85% specificity.[16] In addition to contributing to diagnosis, nCD64 expression measurements can also be used for monitoring sepsis progression. It was found that nCD64 expression declines over time in patients after receiving appropriate medication. On the other hand, patients who did not receive appropriate medication have persistently elevated nCD64 expression.[18] Therefore, measuring nCD64 expression at the point-of-care (POC) could alert the physician about the onset of sepsis as well as monitoring patient condition after administering treatment. Currently used technologies to analyze CD64, such as flow cytometry, are not suited for POC measurements because of instrument size and manual sample preparation.

In order to develop POC biosensors, the use of smartphones as the transducer is gaining interests.[19,20] Likewise, several publications detail microfluidic devices for characterizing and counting cells based on specific cell surface antigen expression. Some of them use smartphone-based systems as detection transducer.[21] However, only a few reports quantify the surface expression of proteins. Zhang *et al.* reported a technique to measure the expression of CD71 from lysed blood samples.[22] The same group expanded this technique to capture highly expressing nCD64 from the blood of septic patients. The capture percentage of cell in septic patients was reported to be significantly higher than that in healthy controls.[23] They also expanded their technique for multiplex capture of CD25, CD64, and CD69 expressing cells in discrete antibody coated regions.[24] The combination of CD64 and CD69 improved sepsis diagnosis with reported area under the ROC curve of 0.98. Although this approach shows diagnostic potential, the requirements for manual off-chip red blood cells (RBC) lysis and a standard bench-top microscope for enumerating the captured cells limits the applicability of this technique at the POC. In order to contribute to developing microfluidic devices suited for POC applications, we recently reported a fully automatic microfluidic biochip for that quantifies a complete white blood cell count (WBC) and nCD64 expression from whole blood.[25] The electrical nature of the device makes it suitable for cost-effective miniaturization, but the process required on-chip RBC lysis prior to WBC analysis.[25]

In this paper, we present a new smartphone-imaged microfluidic biochip to measure CD64 expression on neutrophils. The present device measures nCD64 expression from unprocessed whole blood (does not require RBC lysis), while the smartphone imaging system replaces the standard bench-top microscope for enumerating the captured cells. For capturing the cells, the device uses a microfluidic capture chamber, which has a staggered matrix of pillars coated with anti-CD64 antibody (Fig. 1a). Samples with neutrophils that highly express CD64 travel a shorter distance before getting captured as compared to samples in which neutrophils express lower level of CD64. Based on this property, a statistical model was developed to extract the probability of capture when one neutrophil hits one pillar (ε) and we show that ε increases linearly with CD64 expression (R^2 = 0.82). The applicability of the device to sepsis was demonstrated by analyzing nCD64 from 8 patients suspected of sepsis *versus* time, as they were admitted to the hospital (37 total blood samples). The accuracy of the counting using the developed smartphone-imaged microfluidic biochip was assessed by: (1) counting 8 μm fluorescent beads; (2) using a benchtop fluorescence microscope to compare the beads counting; and (3) using a flow cytometry to compare the nCD64 expression measured with the device.

2. Experimental

2.1. Instrumentation

The flow metering of all required reagents for the capture chamber functionalization and of whole blood and beads through the biochip were performed using a Harvard PHD ULTRA™ pump (Harvard Apparatus, MA, USA). Optical images were taken using a Lumia 1020 smartphone (Nokia, Finland). Fluorescence control measurements were read on a Guava® easyCyte plus flow cytometer (EMD Millipore, USA). Fluorescence from COMPEL™ beads was measured using a BD LSRFortessa™ X-20 cell analyzer (BD Biosciences, USA). PE fluorescent images were taken using a DMI300 B Inverted microscope (Leica, IL, USA). The smartphone-based microscope was calibrated using an Olympus BX63 Upright Microscope. Thickness of the SU-8 structures were measured using an Alpha-Step D-500 Stylus Profilometer (KLA Tencor, CA, USA).

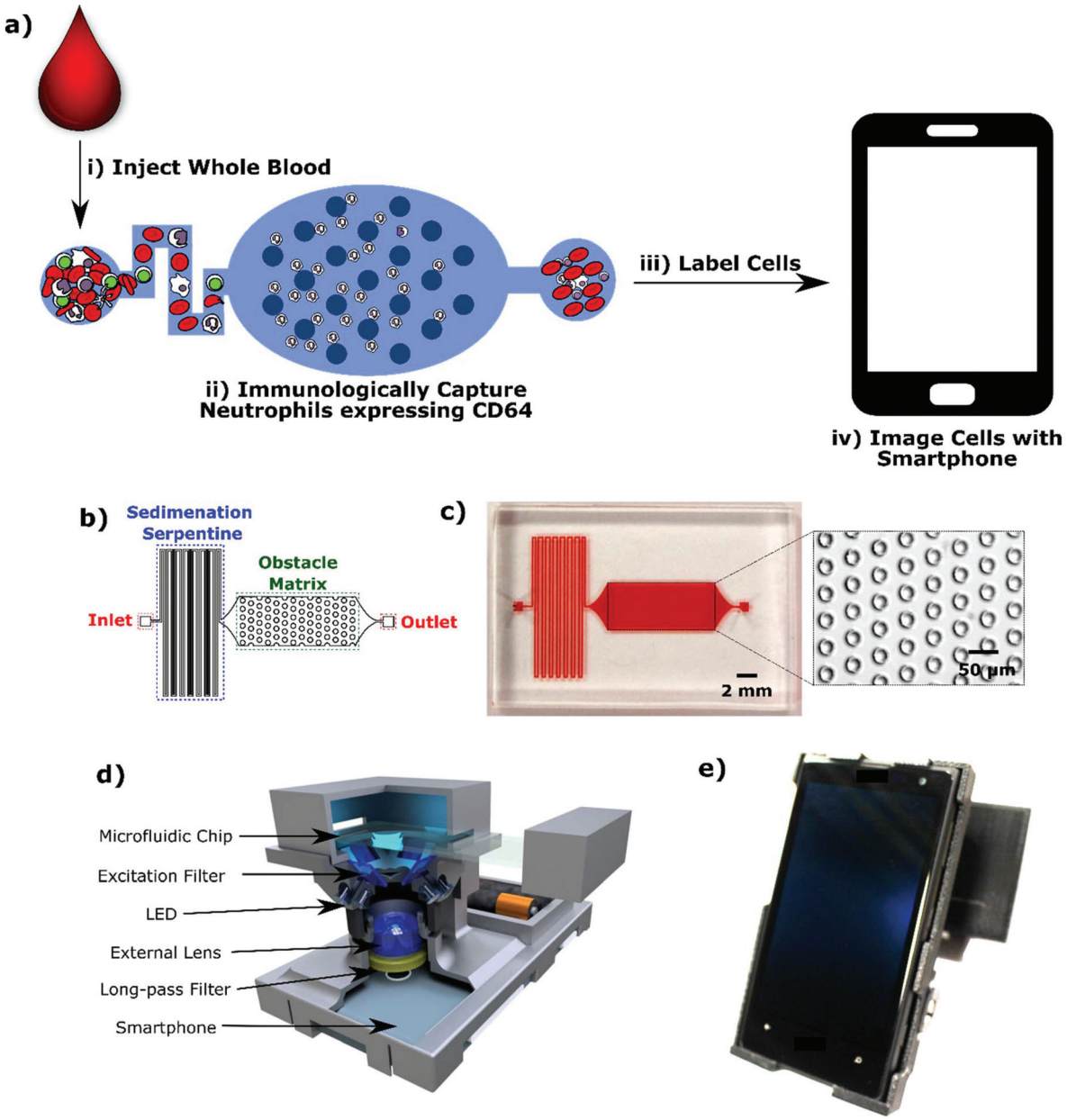

Fig. 1 Assay overview: (a) schematic illustration of the process flow of the assay: (i) whole blood is injected in the chip; (ii) neutrophils expressing CD64 are immunologically captured; (iii) non-specifically bound cells are washed and captured cells labeled with nucleic acid stain, SYTO 16; (iv) the chip is imaged using the smartphone microscope; (b) schematic illustrating the key elements of the microfluidic chip; (c) close-up image of the microfluidic chip. Inset shows the microscopic image of a portion of the obstacle matrix; (d) schematic illustrates the key elements of the smartphone-based fluorescence microscope; (e) isometric view of the smartphone-based microscope.

The layout of the opto-mechanical unit skeleton was drawn using Autodesk Inventor (Autodesk, CA, USA) and the skeleton was printed using a Dimension Elite 3D Printer (Stratasys, MN, USA). Light-emitting-diodes (LEDs, Cat# 516-2800-1-ND) were purchased from Digi-key Electronics (MN, USA). Single band pass filters (Cat# ET470/40x) were from Chroma, USA. The long-pass filter (Cat# FF01-500/LP-23.3-D) was from Semrock, USA. EFL aspherized achromatic lens (Cat# 49-662), and U.S. Air Force hi-resolution target (Cat# 59-152) were from Edmund Optics, USA. The AT205 black aluminum foil tape (Cat# T205-1.0) was from Thorlabs Inc. (NJ, USA). The capture results were analyzed using MatLab (MA, USA).

2.2. Chemicals and reagents

The SU8-50 and SU-8 developer were purchased from MicroChem (MA, USA). Poly(dimethylsiloxane) (PDMS) (SYLGARD 184, Cat# 761036) was purchased from Sigma-Aldrich.

NeutrAvidin protein (Cat# 31000), EZ-Link™ Amine-PEG2-Biotin (Cat# 21346), 2-(*N*-morpholino)ethansulfonic acid (MES)

(Cat# 28390B, EDC (Cat# 22980), NHS (Cat# 24500), SYTO™ 16 green fluorescent nucleic acid stain (Cat# S7578), eBioscience™ 1-step Fix/Lyse solution (10×, Cat# 00-5333-54); ACK lysis buffer (Cat# A1049201), and streptavidin-APC (Cat# SA1005) were purchased from Thermo Fisher Scientific. Bovine Serum Albumin (Cat# A3059) and glycine (Cat# G8898-500G) were purchased from Sigma-Aldrich. Human Fc gamma RI/CD64 Antibody (Cat# MAB1257), and Human Fc gamma RI/CD64 PE-conjugated Antibody (Cat# FAB1257P) were purchased from R&D Systems. COMPEL™ Dragon Green magnetic COOH modified microspheres, 8 μm (Cat# UMDG003), and PE-MESF beads (Cat# 828) were purchased from Bangs Laboratories, Inc., (IN, USA).

2.3. Buffer and solutions

PBS was 0.01 M phosphate buffer, 0.8% (w/v) saline solution and the pH was 7.5. MES was 0.1 M 2-(*N*-morpholino)ethansulfonic acid (pH 6).

2.4. Whole blood samples

Whole blood samples from patients suspected of sepsis (IRB number: 16074) were supplied by Carle Foundation Hospital (Urbana, IL. USA). IRB 16074 was approved by Carle Foundation Institutional Review Board. The recruitment criteria were: (1) patients exhibiting symptoms of infection and inflammation upon arrival to the hospital (through emergency department, walk-ins); (2) ages 18 years and above; (3) all races and genders. Informed consent was obtained for any experimentation with human subjects. Blood from consenting patients was collected in an EDTA tube, then de-identified, and finally stored at 4 °C until use them.

2.5. Microfluidic structures

Microfluidic structures were fabricated with sedimentation serpentines lanes and cell capture chambers with vertical posts. The master mold (negative) of these microfluidics devices was created by a standard SU8-photolithography process using SU8-50 negative photoresist on a Si wafer. The protocol used for the master mold fabrication can be found in the ESI (S-1†). The actual microfluidic structures were made from PDMS, in which elastomer is mixed with curing agent at the ratio of 10 : 1 [w/w] with subsequent pouring on the master mold. After degassing using desiccator, it was cured at 60 °C for 2 h. PDMS channels were cut out using a scalpel and bonded to a glass slide after treating with O_2 plasma.

Both structures, the sedimentation serpentine and capture chamber, were measured to be 55 μm tall. The sedimentation serpentine was 225 mm in length. The capture chamber was designed for containing symmetrically distributed pillars. The pillars were 55 μm tall and 30 μm in diameter, with 18 μm spacing between consecutives pillars. The subsequent pillar rows were staggered with a ratio 0.33. By doing this we ensure that the cells or beads will interact with the pillars more uniformly irrespective of the size.[25] Schematic and optical image of the microfluidic chip can be seen in Fig. 1b and c, respectively.

2.6. Functionalization of the capture chambers

Two different capture agents were functionalized in the capture chamber, depending the purpose of the experiment. Neutravidin was functionalized on the posts in the capture chamber when micro-sized beads were used as control experiments for characterization purposes, and anti-CD64 antibody was functionalized when neutrophils expressing CD64 were intended to be captured. In both cases, the functionalization took place in two steps to modify the capture chambers. First, the chambers were modified with the capture agent (neutravidin or anti-CD64 antibody). Second, BSA was used as blocking agent to minimize non-specific beads/cells capture.

For functionalization of the chamber with neutravidin, the chamber was incubated overnight with a neutravidin solution (100 μg mL^{-1}) at 4 °C. For functionalizing the chamber with anti-CD64 antibody, the chamber was incubated with an antibody solution (100 μg mL^{-1}) overnight at 4 °C. In both cases, immediately before the experiment, the chamber was incubated with a BSA solution (1% BSA in PBS, 1 h at RT).

2.7. Biotin-beads conjugation

COMPEL™ beads (8 μm) were covalently coupled to NH_2–PEG_2–Biotin molecules using slightly modified carbodiimide chemistry.[26,27] The protocol used for the master mold fabrication can be found in the ESI (S-2†).

2.8. Smartphone-based microscope

The design of the smartphone-based microscope is similar to the one that was previously used for the detection of waterborne pathogens.[28,29] In the current work, the existing sample holder was replaced with a new design to easily image cells in multiple microfluidic channels on a microscope slide.

The smartphone-based microscope used a Nokia Lumia 1020 (41 megapixels camera). The skeleton of the opto-mechanical unit was a 3D printed part where the electronic and optical components were incorporated. The unit included eight LEDs to illuminate the sample and excite the fluorophores on the cells. These LEDs are powered with two AA batteries. According to the LEDs datasheet, the maximum power dissipation per LED is 116 mW. If we turn on the LEDs for 5 s, the total energy needed is <1.3 mW h. The spectrum of the LEDs was limited using a single band pass filter. The emitted light is detected using the smartphone rear camera at which a long-pass filter and an external lens (f = 30 mm) were butt-coupled. The inner side of the unit was covered with black aluminum foil to reduce the amount of auto-fluorescence coming from the prototype material. A schematic of the fabricated opto-mechanical unit can be seen in Fig. 1d. Fig. 1e shows an optical image of the smartphone-based microscope.

2.9. Biochip measurement procedure

The entire biochip measurement procedure included: (1) sample injection and cell immunocapture; (2) cell staining; and (3) imaging and counting analysis. All previous steps were performed on-chip. The entire procedure is summarized in

Fig. 1a. When using beads for characterization experiments, step 2 is not necessary.

2.9.1. Sample injection and cells immunocapture. A syringe (loaded with the whole blood sample) was connected to the sedimentation serpentine leading to the capture chamber (previously functionalized with AbCD64). The sample (1 μL) was injected in the capture chamber at 1 μL min^{-1} (max flow velocity inside the chamber = 290.8 μm s^{-1}). No incubation time was needed for capturing neutrophils expressing CD64. Immediately after, the non-specifically captured cells were washed out by flushing the channel with 1% BSA in PBS (50 μL, 10 μL min^{-1}).

When biotinylated beads were used, the same protocol was executed. However, in this case, the injected sample was a solution containing 1000 beads (flow rate: 25 μL min^{-1}) and the capture chamber was previously functionalized with neutravidin.

2.9.2. Cells staining. In order to image the cells using the smartphone, the captured cells were labeled with a nucleic acid stain (SYTO™ 16). Before the staining, the captured cells were first fixed by flowing 1-step fix/lyse solution (1×, 50 μL, 10 μL min^{-1}). The fix solution was incubated for 15 min. In addition to fixing cells, this solution also lyses RBCs that might be remaining in the channel. After the fix solution incubation, a SYTO™ 16 solution (2 μM, 1% BSA in PBS) was injected in the capture chamber (50 μL, 10 μL min^{-1}). Before the imaging, the SYTO™ 16 solution was incubated in the dark (15 min). When biotinylated beads were used, the staining step was not required as the beads were already fluorescent.

2.9.3. Imaging and counting analysis. The smartphone-based microscope used a Nokia Lumia 1020. The regular camera application of the smartphone allows to adjust white balance, focus, ISO, and exposure time settings of an image, and capture a high-resolution raw format image (*i.e.* DNG, 5360 × 7152 pixels) as well as a low-resolution image (*i.e.* JPG, 1936 × 2592 pixels) at a single shot. For imaging cells, daylight mode was used for white balance and the imaging plane was found by autofocusing. ISO was set at 100 and exposure time was set at 4 s. For imaging beads, same settings were used but the exposure time was 1 s.

After imaging the chamber, the data was transferred to a computer for analysis. First, background was subtracted from raw, grayscale images. Then, the images were binarized by performing a thresholding operation. Finally, using a transform operation from the MATLAB library, cells were identified from the binary image. The sequence of operation for extracting cell-coordinates can be seen in the ESI (S-3†).

2.10. CD64 expression control measurements

In order to validate the results obtained using the developed smartphone-imaged microfluidic biochip, the same patient samples analyzed with our device were analyzed using a flow cytometry. Flow cytometry was used as reference gold standard method for measuring CD64 expression of neutrophils in the whole blood samples. To do this, 8 μL whole blood was mixed with an AbCD64-PE solution (30 μL, 10-fold from stock, in 0.5% BSA), and incubated in the dark (30 min). After the incubation, red blood cells were lysed by adding 160 μL ACK lysis buffer (15 min incubation in the dark). Then, 3× PBS (80 μL) was added. Finally, fluorescence from the cells was recorded using appropriate settings on the flow cytometer. To account for laser intensity variation of the flow cytometer, the fluorescence of PE-MESF beads was used to normalize the fluorescence of the blood samples.

3. Results and discussion

3.1. Smartphone image resolution and calibration

The resolution of the image provided by the smartphone-based microscope must be good enough to distinguish individual cells (10–12 μm size). The resolution of the smartphone camera was assessed imaging a U.S. Air Force (USAF) hi-resolution target. The USAF target consists of 51 elements with logarithmically increasing spatial frequency of lines within each element. The highest resolvable element determines the resolution of the imaging set-up. In the captured image (Fig. 2a), three distinct peaks corresponding to three horizontal and vertical elements (Group 6 Element 3) can be appreciated. From this image the spatial resolution was calculated to be 6.2 μm, which was considered sufficient for imaging single cells. This resolution was assessed imaging 8 μm fluorescent beads. As it can be seen in Fig. 2b, individual 8 μm beads are clearly distinguishable in the image acquired by the smartphone-based microscope.

The calibration of the smartphone-based microscope was performed by counting the 8 μm fluorescent beads with the developed device and with a regular benchtop microscope (Olympus BX63 Upright Microscope, 10× objective lens (NA = 0.25), FITC filter set). The benchtop microscope was used as a reference method. Several chambers with different number of captured beads (in a range from 500 to 4500) were imaged using both systems and the beads were then counted using the procedure explained in section 2.9.3. Fig. 2c compares the number of beads counted using both systems. As it can be seen, a very good agreement between the two methods was obtained ($y = 0.94x + 5.6$, $R^2 = 0.99$). These data suggest that the bench top microscope could be substituted by the developed smartphone-based microscope for counting cells.

3.2. Assessment of the bioactivity of the biotinylated beads

The biofunctionality of the homogenous biohybrid particles (biotin-beads) was initially assessed using a flow cytometry. For this purpose, 6 batches of beads were conjugated to different NH_2–PEG_2–biotin concentrations (0, 10, 50, 100, 500, and 1000 μg mL^{-1}) using the procedure described in section 2.7. After the biotin conjugation, streptavidin-APC molecule was also added to give fluorescent properties to the beads. The fluorescence of the beads was interrogated using a BD LSRFortessa™ X-20 flow cytometer. The results of the fluo-

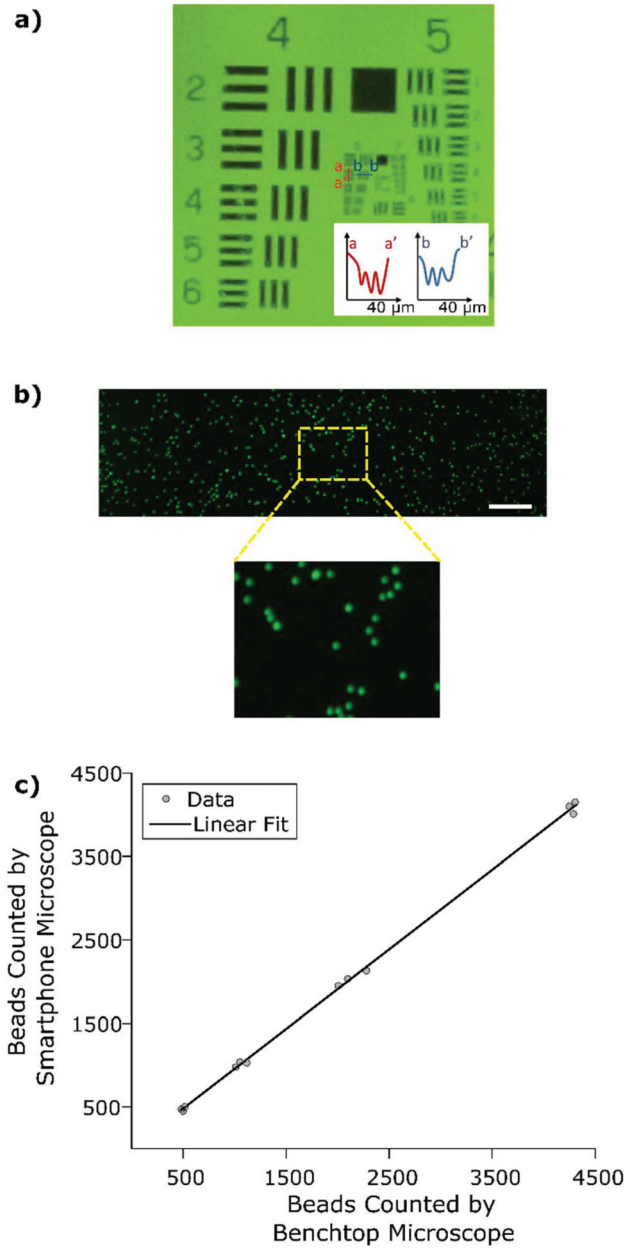

Fig. 2 Smartphone microscope characterization: (a) image of a U.S. Air Force resolution chart captured using the smartphone-based microscope. The smallest resolvable element is Group 6 Element 3. Hence, the spatial resolution of the imaging set-up is 6.2 μm. Subplots are showing the pixel resolution of the image for the cross sections of (a–a′) and (b–b′) for vertical and horizontal lines of G6E3, respectively; (b) an image of 8 μm fluorescent beads in the microfluidic channel acquired using the mobile microscope. Scale bar: 1 mm; (c) comparison of the bead counts of different samples obtained from a benchtop fluorescence microscope to that of our smartphone-based microscope. Each data point is a single measurement. There is good agreement between the two counts ($y = 0.94x + 5.6$, $R^2 = 0.99$, $p < 0.0001$).

rescence analysis can be seen in Fig. 3a. Histograms shows clear and sharp distributions of the fluorescence for all populations. Also, the median fluorescence intensities (MFI) of each population are very well distinguishable.

3.3. Principle of the probability of capture per collision

The microfluidic biochip was designed to predict the surface biomolecule density on cells and micron sized beads based on the probability of capture per collision.

The fraction of captured cells or beads (γ) in the capture chamber is a function of the channel distance and it is also affected by the biomolecule density on the surface of the captured element.[26,30] Thus, the probability of neutrophil capture on a pillar increases with increasing the CD64 density and the probability of micro-sized beads capture on a pillar increases with increasing the biotin density. Likewise, γ can be used to obtain the probability of capture per collision with the pillar (ε) as it can be seen in eqn (1).

$$\gamma = 1 - (1 - \varepsilon)^{\frac{x}{\Delta x}} \quad (1)$$

In eqn (1), Δx is the downstream distance between consecutive pillars that a cell collides. Therefore, at a distance x, a cell will encounter $x/\Delta x$ pillars. A key condition is that Δx is constant. The capture chamber was designed to satisfy this condition. Thus, in the obstacle matrix, each row is shifted laterally with respect to the previous row by a distance equal to a third of the center-to-center distance between pillars in the same row, giving rise to a cyclic spatial geometry of pillars.[26,30] In such a cyclic geometry which is repeated every 3 rows, distance between two pillars (g) is 18 μm and the diameter of each pillar (d) is 30 μm. Therefore $\Delta x = 3(d + g) = 144$ μm.

Based on this, in this paper ε will be used as a figure of merit to analyze the CD64 density on neutrophils. Variation of cell fraction with distance is obtained experimentally by imaging the chip with the smartphone set-up. Eqn (1) is fitted to the distribution of captured cells in the channel to obtain ε. A custom image processing algorithm was written in MatLab to extract the coordinates of cells from the images. These coordinates were used to generate the experimental distribution of cumulative density of cells with distance. Then, the theoretically expected cumulative distribution was fitted to the experimental data to extract ε.

In order to facilitate imaging, cells were passively brought in one plane. This is why the capture chamber was preceded by a sedimentation serpentine section. The white blood cells slowly sedimented in the sedimentation serpentine under the effect of gravity as they flowed through it. It was determined that the 55 μm tall channel, which is 225 mm in length, is sufficiently long for the white blood cells to sediment in the flow.[31]

3.4. Assessment of the functionality of the smartphone-imaged microfluidic biochip

The ability of the smartphone-imaged microfluidic biochip to develop spatial profiles and to predict surface densities was assessed by using biotinylated beads. Biotinylated beads were used as a model before working with cells. These beads were selected as a model because: (1) their similar size to the neutrophils; and (2) the biotin surface density was known.

Biotinylated beads with different surface densities were injected in the microfluidic biochip as described in section

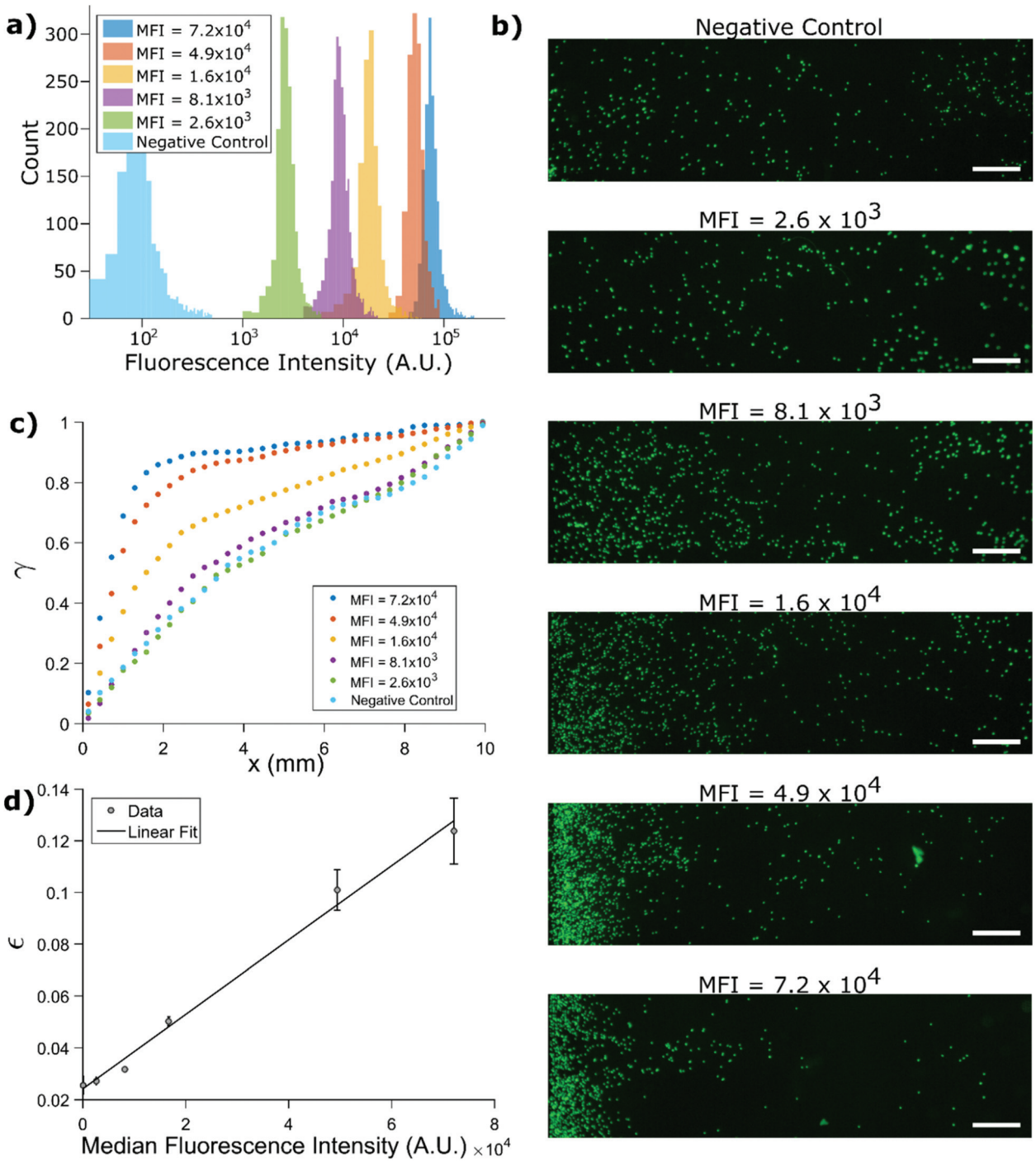

Fig. 3 Measuring surface density of biotin on beads using a smartphone microscope: (a) histograms showing the fluorescence of streptavidin-APC measured by a flow cytometer. Legend shows the measured Median Fluorescence Intensity (MFI); (b) smartphone based microscope images of microbeads captured on the microfluidic chip with increasing surface density of biotin. Beads are injected from left to right. Scale bar: 1 mm; (c) plot shows fraction of beads captured, γ, as a function of distance traveled in the channel, x; (d) plot shows the measured probability of capture per collision, ε, *versus* red fluorescence measured by flow cytometry (R^2 = 0.99).

2.9.1. The spatial profiles of captured beads were imaged using the smartphone-based microscope. Representative examples of the profiles acquired using the smartphone-based microscope can be seen in Fig. 3b. Profiles of captured beads correlate the distance from the inlet where the beads were captured to the beads surface biotin density. Higher accumulation of beads close to the inlet were obtained for higher biotin densities. This effect can be also appreciated in Fig. 3c where the cumulative fraction of captured beads (γ) increased more rapidly for higher MFI. Although eqn (1) predicted a steady

increase to saturation, this plot shown an inflection point around 2 mm. Also, the inflection point was more pronounced for higher MFIs. This could be attributed to some non-specific beads capture due to the accumulation of beads in the initial rows when high density of specific capture was obtained. Finally, ε was calculated. Fig. 3d plots the probability of capture against the MFI. In accordance with Fig. 3b, ε increased linearly with the fluorescence intensity (R^2 = 0.99). Larger error bars for higher MFIs could also indicate the same non-specific beads capture effect.

3.5. Assessment of the specific capture of neutrophils expressing CD64

To validate our analysis, it is important to demonstrate the captured cells on the capture chamber are cells expressing CD64. In order to test the specificity of the cell capture, captured cells were labelled with AbCD64-PE. The fluorescence of the PE was analyzed using an inverted benchtop microscope. As expected, most of the captured cells showed fluorescence after labelling (Fig. 4a). By this technique, the specificity of cell capture was estimated at around 96%.

3.6. Prediction of nCD64 from whole blood patient samples based on the capture chamber spatial profile

The ability of the smartphone-imaged microfluidic biochip to predict the expression of CD64 on neutrophils was assessed by analyzing the capture chamber spatial profiles using the same procedure demonstrated for biotinylated beads in section 3.4.

In these experiments, 37 whole blood samples collected from 8 patients were injected in the biochip as described in section 2.9.1. to specifically capture neutrophils expressing CD64. Then, the SYTO™ 16 staining procedure from section 2.9.2. was followed. Afterwards, the spatial distribution of captured cells was obtained by imaging the capture chamber with the smartphone-based microscope. Representative examples of the spatial profiles acquired using the smartphone-based microscope can be seen in Fig. 4b. Similar as the results obtained in section 3.4., profiles of captured cells clearly show correlation between the distance from the inlet where the cells were captured and the expression of CD64 on the cells surface. The same samples used in these experiments were also analyzed using a flow cytometry (reference method) to calculate the CD64 expression following the procedure described in section 2.10.

As CD64 increases, the neutrophils become more likely to be captured when they hit a pillar. Consequently, the mean distance traveled by the captured neutrophils is shorter for neutrophils expressing higher levels of CD64. This behavior is also reflected in γ (Fig. 4c). Similar to the bead capture, the fraction of cells captured increased more rapidly with distance for samples which have higher CD64 expression. However, in this case, eqn (1) better represented the data as the inflection point was not clearly identified. A possible explanation could be the soft biophysical nature of the cells which prevent aggregation as compared to beads.

Finally, ε was also calculated. Fig. 4d plot the probability of capture against the CD64 expression measured from flow cytometry. In accordance with Fig. 4b, ε increased linearly with the CD64 expression. A correlation coefficient R^2 = 0.82 was obtained for the 37 analyzed samples, demonstrating a good linear correlation.

3.7. Application of the smartphone-imaged microfluidic biochip for time course analysis of patient samples

The smartphone-imaged microfluidic biochip developed was applied to track the nCD64 expression level in 8 patients *versus* time during their stay in the Carle Foundation Hospital. The obtained data was added to other relevant patient information such as age, blood culture test results, sepsis diagnosis, *etc*. This data is summarized on Table S-1,† which can be found in the ESI (S-4†).

For this analysis, first, data from Fig. 4d was used to obtain CD64 expression from the biochip analysis. Thus, a threefold cross-validation with 1000 random sample selection was performed on the ε and control data from flow cytometry. By this technique Fig. 5a was generated. In this plot expression measurements were color-coded to denote the 8 patients included in the study. A correlation coefficient R^2 = 0.82 (slope = 0.99) was obtained for the 37 analyzed samples, demonstrating a good linear correlation. It is important to note that for the data shown in Fig. 4d and 5a, the apparent high variability for low nCD64 expression (below ~1.5) is less important and does not impact the measurement results as these low expressions generally represent patients in the healthy state. Whereas, the higher nCD64 expression over about 1.5 is more relevant for disease management. In addition to the correlation, the agreement between the expressions obtained by both methods was also tested using the Bland–Altman plot (Fig. 5b). As can be seen in the plot, most of the analyzed samples (36) were well in between the limits of agreement. Finally, Fig. 5c plots the nCD64 expression measured for different patients during the time they were admitted in the hospital. As expected, the profiles are different for each patient. Some interesting relationships are found when comparing this data with the data provided by the hospital (Table S-1†). For instance, patient G (yellow) had a negative blood culture, was not diagnosed with sepsis and showed a steady and low CD64 expression. On the other hand, patient E, which was diagnosed with Gram negative septicemia, expressed very high CD64. However, during the stay of the patient in the hospital, the expression decreased dramatically. As can also be noted, that 6 of the 8 patients had negative blood cultures also highlighting the importance of developing approaches for immune profiling as in this paper, in addition to the critical need for rapid detection of the bacterial or viral pathogens.[1,11]

The total time for measurement and analysis and the ease of measurement are both very important to consider. All steps prior to the measurement including fabrication and functionalization can be considered as part of the cartridge/biochip fabrication and preparation and in a practical setting, as the functionalized devices would be provided to the user in

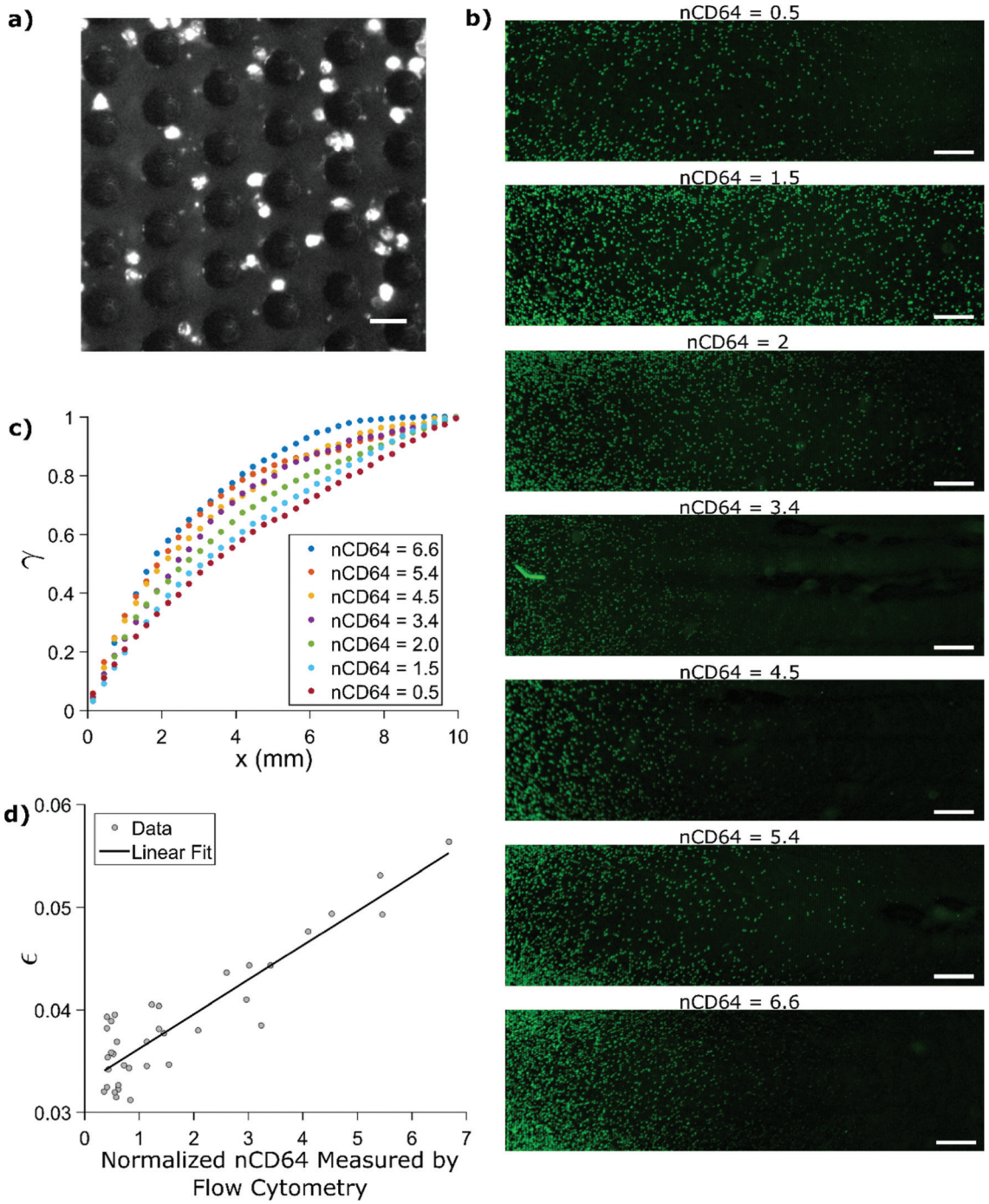

Fig. 4 Measuring nCD64 expression using a smartphone microscope: (a) microscopic image of immunologically captured white blood cells on the pillars. Cells are labeled with PE conjugated anti-CD64 antibody (scale bar: 20 μm); (b) images show the profiles of captured white blood cells with increasing CD64 expression. Whole blood was injected from left to right. As nCD64 increases, cell capture shifts to the left. Scale bar: 1 mm; (c) plot shows fraction of cells captured, γ, as a function of distance traveled in the channel, x; (d) plot shows the measured probability of capture per collision, ε, *versus* nCD64 measured by flow cytometry for 37 patient samples ($R^2 = 0.82$, $y = 0.0034x + 0.0329$, $p < 0.0001$). Each data point is a single measurement.

a dry packaged condition. From injection of whole blood into the cartridge, the total time for the measurement is <50 min in the following steps: (1) sample injection and cell immunocapture (1 μL, 1 min); (2) wash step (1% BSA in PBS, 50 μL, 5 min); (3) cells fixation (1-step fix/lyse solution, 50 μL, 5 min, incubation time: 15 min); (4) cells staining (2 μM SYTO™ 16, 50 μL, 5 min, incubation time: 15 min); (5) imaging (30 s); and (6) counting analysis (30 s). This procedure is summarized in ESI (S-5†). We envision all reagents to be used for blood flow and cell labeling to be packaged in pouches in a one-time-use

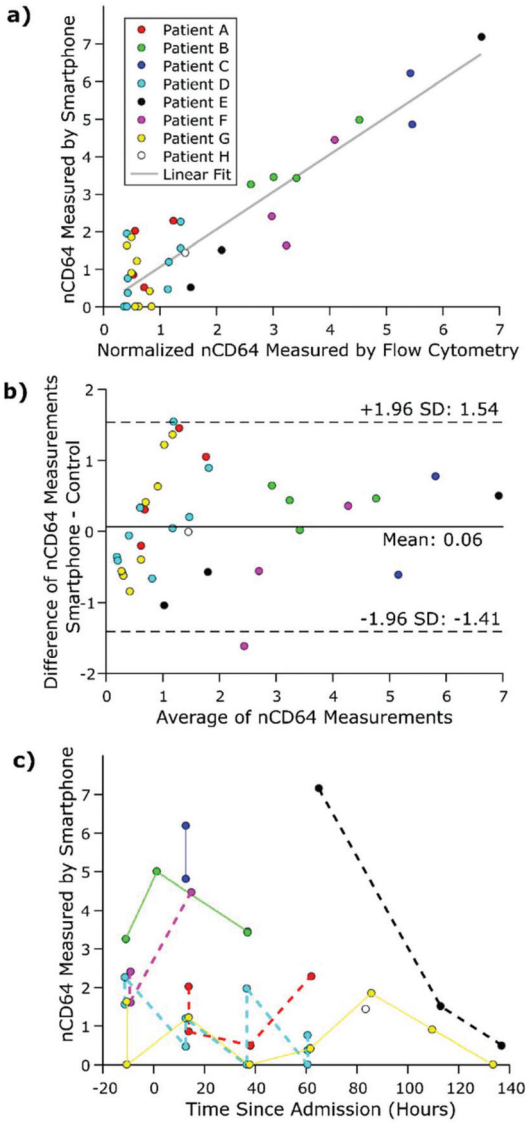

Fig. 5 Time course measurements: (a) plot compares patient-wise nCD64 expression measured using the smartphone-based microscope to the control measurements performed using flow cytometry. There is good correlation between the two measurements (R^2 = 0.82, y = 0.99x + 0.07, p < 0.0001); (b) Bland–Altman analysis showing all but one nCD64 measurements using the mobile microscope are within two standard deviations of the mean difference. The variability in our measurements is less for high nCD64 expression representing sicker patients; (c) plot shows nCD64 expression in patients tracked over time since they were admitted to the hospital. Each color denotes a unique patient (single measurement). Color legend same as panel (a). Patients A, D, E, F, and H were diagnosed with sepsis. Data from these patients is plotted with bold, dashed lines. Some data-points are close so they are hard to distinguish on the plot and coincide.

cartridge and the reader to also contain the pneumatics to push the reagents in the cartridge. The compact form factor of the optical reader instrument with the smartphone camera-based microscope, and the one time use cartridge, makes the approach very attractive to be used at various point-of-care settings.

4. Conclusions

Rapid and continuous measurement of CD64 expression on neutrophils at the patient bedside could be useful in predicting the onset of sepsis as well monitoring the response of patients to medication. In this paper, a portable smartphone-imaged microfluidic biochip capable of measuring CD64 expression from minute quantities of blood was described. The developed biochip uses unprocessed whole blood. The system was first characterized using biotinylated beads as a model. The robustness and the applicability of the device was demonstrated by analyzing 37 blood samples from 8 patient admitted in the Carle Foundation Hospital, with the samples in the range of physiologically relevant CD64 expression. The portable nature of the imaging set-up and the simplicity of our assay make it suitable for translating it to a point-of-care technology. If deployed in the hospital, we believe this technology has the potential to significantly contribute in the sepsis diagnosis.

Conflicts of interest

There are no conflicts of interest to declare.

Author contribution

T. G. and R. B. conceptualized the study. E. V., T. G., H. C. K., J. B., G. L. D., A. O., and R. B. wrote and edited the paper. H. C. K. built and characterized the smartphone-microscope and H. C. K. and T. G. performed the optimization. E. V. and J. B. performed experiments related to functionalizing the beads. C. G. performed the bead capture experiments. C. G., N. N., and J. T. fabricated the microfluidic channels for the experiments. A. G. provided intellectual input and feedback on study design. U. H. provided intellectual input and feedback on data analysis.

References

1 M. Singer, C. S. Deutschman, C. W. Seymour, M. Shankar-Hari, D. Annane, M. Bauer, *et al.*, The Third International Consensus Definitions for Sepsis and Septic Shock (Sepsis-3), *J. Am. Med. Assoc.*, 2016, **315**(8), 801–810.
2 J.-L. Vincent, J. C. Marshall, S. A. Ñamendys-Silva, B. François, I. Martin-Loeches, J. Lipman, *et al.*, Assessment of the worldwide burden of critical illness: the Intensive Care Over Nations (ICON) audit, *Lancet Respir. Med.*, 2014, **2**(5), 380–386.
3 C. Fleischmann, A. Scherag, N. K. J. Adhikari, C. S. Hartog, T. Tsaganos, P. Schlattmann, *et al.*, Assessment of Global Incidence and Mortality of Hospital-treated Sepsis. Current Estimates and Limitations, *Am. J. Respir. Crit. Care Med.*, 2016, **193**(3), 259–272.

4 C. M. Torio and B. J. Moore, *National Inpatient Hospital Costs: The Most Expensive Conditions by Payer, 2013*, Agency for Healthcare Research and Quality, Rockville, MD, 2016, HCUP Statistical Brief #204.
5 W. J. Wiersinga and C. W. Seymour, *Handbook of Sepsis*, Springer International Publishing, 2018, vol. VIII, 267 p.
6 P. E. Marik and A. M. Taeb, SIRS, qSOFA and new sepsis definition, *J. Thorac. Dis.*, 2017, **9**(4), 943–945.
7 A. Kalantari, H. Mallemat and S. D. Weingart, Sepsis Definitions: The Search for Gold and What CMS Got Wrong, *West. J. Emerg. Med.*, 2017, **18**(5), 951–956.
8 A. Kumar, D. Roberts, K. E. Wood, B. Light, J. E. Parrillo, S. Sharma, *et al.*, Duration of hypotension before initiation of effective antimicrobial therapy is the critical determinant of survival in human septic shock, *Crit. Care Med.*, 2006, **34**(6), 1589–1596.
9 J. Phua, W. J. Ngerng, K. C. See, C. K. Tay, T. Kiong, H. F. Lim, *et al.*, Characteristics and outcomes of culture-negative versus culture-positive severe sepsis, *Crit. Care*, 2013, **17**(5), R202.
10 C. Rhee, R. Dantes, L. Epstein, D. J. Murphy, C. W. Seymour, T. J. Iwashyna, *et al.*, Incidence and Trends of Sepsis in US Hospitals Using Clinical vs Claims Data, 2009–2014, *J. Am. Med. Assoc.*, 2017, **318**(13), 1241–1249.
11 B. Reddy Jr., U. Hassan, C. Seymour, D. C. Angus, T. S. Isbell, K. White, *et al.*, Point-of-care sensors for the management of sepsis, *Nat. Biomed. Eng.*, 2018, **2**, 640–648.
12 C. Wacker, A. Prkno, F. M. Brunkhorst and P. Schlattmann, Procalcitonin as a diagnostic marker for sepsis: a systematic review and meta-analysis, *Lancet Infect. Dis.*, 2013, **13**(5), 426–435.
13 P. Póvoa, L. Coelho, E. Almeida, A. Fernandes, R. Mealha, P. Moreira, *et al.*, C-reactive protein as a marker of infection in critically ill patients, *Clin. Microbiol. Infect.*, 2005, **11**(2), 101–108.
14 S. Harbarth, K. Holeckova, C. Froidevaux, D. Pittet, B. Ricou, G. G. Grau, *et al.*, Diagnostic Value of Procalcitonin, Interleukin-6, and Interleukin-8 in Critically Ill Patients Admitted with Suspected Sepsis, *Am. J. Respir. Crit. Care Med.*, 2001, **164**, 396–402.
15 S. Li, X. Huang, Z. Chen, H. Zhong, Q. Peng, Y. Deng, *et al.*, Neutrophil CD64 expression as a biomarker in the early diagnosis of bacterial infection: a meta-analysis, *Int. J. Infect. Dis.*, 2014, **17**(1), e12–e23.
16 J. Cid, R. Aguinaco, R. Sánchez, G. García-Pardo and A. Llorente, Neutrophil CD64 expression as marker of bacterial infection: A systematic review and meta-analysis, *J. Infect.*, 2010, **60**(5), 313–319.
17 J. Du, L. Li, Y. Dou, P. Li, R. Chen and H. Liu, Diagnostic Utility of Neutrophil CD64 as a Marker for Early-Onset Sepsis in Preterm Neonates, *PLoS One*, 2014, **9**(7), e102647.
18 A. Dimoula, O. Pradier, Z. Kassengera, D. Dalcomune, H. Turkan and J.-L. Vincent, Serial Determinations of Neutrophil CD64 Expression for the Diagnosis and Monitoring of Sepsis in Critically Ill Patients, *Clin. Infect. Dis.*, 2014, **58**(6), 820–829.
19 J. Guo and X. Ma, Simultaneous monitoring of glucose and uric acid on a single test strip withdual channels, *Biosens. Bioelectron.*, 2017, **94**, 415–419.
20 J. Guo, Smartphone-Powered Electrochemical Dongle for Point-of-Care Monitoring of Blood β-Ketone, *Anal. Chem.*, 2017, **89**, 8609–8613.
21 M. K. Kanakasabapathy, H. J. Pandya, M. S. Draz, M. K. Chug, M. Sadasivam, S. Kumar, *et al.*, Rapid, label-free CD4 testing using a smartphone compatible device, *Lab Chip*, 2017, **17**, 2910–2919.
22 Y. Zhang and D. Pappas, Microfluidic cell surface antigen expression analysis using a single antibody type, *Analyst*, 2016, **141**, 1440–1447.
23 Y. Zhang, W. Li, Y. Zhou, A. Johnson, A. Venable, A. Hassan, *et al.*, Detection of sepsis in patient blood samples using CD64 expression in a microfluidic cell separation device, *Analyst*, 2018, **143**, 241–249.
24 Y. Zhang, Y. Zhou, W. Li, V. Lyons, A. Johnson, A. Venable, *et al.*, Multiparameter Affinity Microchip for Early Sepsis Diagnosis Based on CD64 and CD69 Expression and Cell Capture, *Anal. Chem.*, 2018, **90**(12), 7204–7211.
25 U. Hassan, T. Ghonge, B. Reddy Jr., M. Patel, M. Rappleye, I. Taneja, *et al.*, A point-of-care microfluidic biochip for quantification of CD64 expression from whole blood for sepsis stratification, *Nat. Commun.*, 2017, **8**, 15949.
26 T. Ghonge, A. Ganguli, E. Valera, M. Saadah, G. L. Damhorst, J. Berger, *et al.*, A microfluidic technique to estimate antigen expression on particles A microfluidic technique to estimate antigen expression on particles, *APL Bioeng.*, 2017, **1**(1), 016103.
27 E. Valera, J. Berger, U. Hassan, T. Ghonge, J. Liu, M. Rappleye, *et al.*, A microfluidic biochip platform for electrical quantification of proteins, *Lab Chip*, 2018, **18**, 1461–1470.
28 H. C. Koydemir, Z. Gorocs, D. Tseng, B. Cortazar, S. Feng, R. Y. L. Chan, *et al.*, Rapid imaging, detection and quantification of Giardia lamblia cysts using mobile-phone based fluorescent microscopy and machine learning, *Lab Chip*, 2015, **15**, 1284–1293.
29 H. C. Koydemir, S. Feng, K. Liang, R. Nadkarni, P. Benien and A. Ozcan, Comparison of supervised machine learning algorithms for waterborne pathogen detection using mobile phone fluorescence microscopy, *Nanophotonics*, 2017, **6**(4), 731–741.
30 D. W. Inglis, J. A. Davis, R. H. Austin and J. C. Sturm, Critical particle size for fractionation by deterministic lateral displacement, *Lab Chip*, 2006, **6**, 655–658.
31 T. Tachi, N. Kaji, M. Tokeshi and Y. Baba, Simultaneous Separation, Metering, and Dilution of Plasma from Human Whole Blood in a Microfluidic System, *Anal. Chem.*, 2009, **81**, 3194–3198.